

## A closed-form, analytical approximation for apparent surface charge and electric field of molecules.

Dan Folescu<sup>1</sup> and Alexey V. Onufriev<sup>1, 2, 3, a)</sup>

<sup>1)</sup>*Department of Computer Science, Virginia Tech*

<sup>2)</sup>*Department of Physics, Virginia Tech*

<sup>3)</sup>*Center for Soft Matter and Biological Physics, Virginia Tech, Blacksburg, VA 24061, USA*

Closed-form, analytical approximations for electrostatic properties of molecules are of unique value, as these can provide computational speed, versatility, and physical insight. Here, we derive a simple, closed-form formula for the apparent surface charge (ASC), as well as for the electric field, generated by a molecular charge distribution in aqueous solution. The approximation, with no fitted parameters, is tested against numerical solutions of the Poisson equation, where it yields a significant speed-up. For neutral small molecules, the hydration free energies estimated from the closed-form ASC formula are within 0.8 kcal/mol RMSD from the numerical Poisson reference; the electric field at the surface is in quantitative agreement with the reference. Performance of the approximation is also tested on larger structures, including a protein, a DNA fragment, and a viral receptor-target complex. For all structures tested, a near quantitative agreement with the numerical Poisson reference is achieved, except in regions of high negative curvature, where the new approximation is still qualitatively correct. A unique efficiency feature of the proposed "source-based" closed-form approximation is that the ASC and electric field can be estimated individually at any point or surface patch, without the need to obtain the full global solution. An open source software implementation of the method is available: <http://people.cs.vt.edu/~onufriev/CODES/aasc.zip>.

---

<sup>a)</sup>Electronic mail: alexey@cs.vt.edu

# I. INTRODUCTION

Accurate and efficient modeling of solvation effects at the atomistic level is a critical component of modern efforts to understand molecular structure and function<sup>1-5</sup>. Analysis and visualization of electrostatic properties of biomolecules, including the electric field and surface charge generated by the molecular charge distribution, have made an impact in qualitative reasoning about biomolecules<sup>1,6</sup>.

There are two broad approaches to the modeling of molecular electrostatics and solvation effects: explicit and implicit solvation methods<sup>7</sup>. Arguably the most widely used model of solvation is that for which individual solvent molecules are treated explicitly, on the same footing with the target molecule. However, accuracy of the explicit solvent representation comes at high price, computationally, limiting the practical utility of atomistic simulations in many areas. The implicit, continuum solvation approach – treating solvent as a continuum with the dielectric and non-polar properties of water – can offer much greater effective simulation speeds compared to the explicit solvent models<sup>8-18</sup>. The Poisson equation<sup>9,10,19-23</sup> of classical electrostatics<sup>24</sup> provides an exact formalism – within the continuum, local, linear-response dielectric approximation of solvent in the absence of mobile ions – for computing the electrostatic potential  $V(\mathbf{r})$  produced by a molecular charge distribution  $\rho(\mathbf{r})$  characterizing the solute:

$$\nabla\epsilon(\mathbf{r})\nabla V(\mathbf{r}) = -4\pi\rho(\mathbf{r}), \quad (1)$$

where  $\epsilon(\mathbf{r})$  is the dielectric constant. Once  $V(\mathbf{r})$  is obtained, the electrostatic part of the solvation free energy is easily computed<sup>24</sup>.

The problem of finding  $V(\mathbf{r})$  is mathematically equivalent<sup>25,26</sup> to finding a continuous charge density,  $\sigma$ , on the dielectric boundary (DB), such that:

$$V(\mathbf{r}) = \sum_i \frac{q_i}{|\mathbf{r} - \mathbf{r}_i|} + \oint_{\partial S} \frac{\sigma(\mathbf{s})}{|\mathbf{r} - \mathbf{s}|} d^2s, \quad (2)$$

where  $\rho(\mathbf{r})$  is the discrete charge distribution, formed by  $n$  point charges  $q_1, \dots, q_n$ , and  $\sigma(\mathbf{s})$  is the *apparent surface charge* (ASC) associated with each surface patch  $\mathbf{s}$ . The second term in the above equation represents the so-called reaction field potential<sup>27-29</sup>. Conceptually, once the ASC,  $\sigma(\mathbf{s})$ , is found, all of the solvation effects, at the level of the Poisson equation, can be computed. A great variety of practical, widely used methods, including multiple



modern derivatives of PCM<sup>25</sup> and COSMO<sup>30</sup>, utilize this general idea – the apparent surface charge (ASC) formalism, see Refs.<sup>31,32</sup> for comprehensive reviews.

The reformulation of the Poisson problem via equation 2 has a number of technical advantages made apparent over the years, especially in quantum mechanical (QM) calculations<sup>8,32</sup>.

A number of ASC-based methods yield numerically exact solutions to the Poisson equation, in the sense that the exact solution can, at least in principle, be approximated with an arbitrary precision. Formally exact, linear-scaling implementations of numerical ASC methods, based on conjugate gradient or domain decomposition, exist<sup>32</sup>. Concerns related to computational cost of numerically exact approaches<sup>31</sup> have led to the development of approximate ASC-based methods, such as the widely used COSMO<sup>30</sup>, GCOSMO<sup>33</sup>, and C-PCM<sup>34</sup>. These methods rely on approximations to equation 2. Still, even these approximate ASC-based methods employ a significant numerical component, such as numerical matrix inversion, which may carry appreciable computational overhead, especially as the structure size grows<sup>35,36</sup>. Therefore, in applications where computational efficiency and algorithmic simplicity is paramount, numerical ASC-based methods may not be as competitive as approximations to the Poisson equation based purely on closed-form analytical expressions<sup>27</sup>.

Among the fully analytical approximations to the Poisson equation, the generalized Born (GB) model<sup>8,37–65</sup> is arguably the most widely used, especially in atomistic simulations<sup>66–76</sup>. However, despite its multiple documented success stories<sup>77</sup> the GB model does not have the versatility of equation 2, and the associated benefits of an ASC-based formulation of biomolecular electrostatics. Here we aim to fill the gap by deriving an *analytical*, closed form approximation to the Poisson equation for the ASC and the (normal) electric field around an arbitrary shaped molecule. Standard numerical solutions of the Poisson equation are used as the reference. We refrain from comparisons with well-established, optimized numerical implementations of ASC methods in this initial investigation.

The outline of the paper is as follows. Section II describes computational testing materials and methodology. Section III is focused on our analytical ASC approximation: we first derive an exact analytical ASC reference on a sphere (III A), and present our approximate form of the ASC for arbitrary molecular geometries (III B). We test the approximate ASC against the exact analytical ASC reference using a spherical test case (III C), which simulates relevant electrostatic configurations that we will encounter in later sections. Application of our model to solvation energy calculations is presented in section III D. Numerical performance

and accuracy analysis, along with an example applications are presented in section IV, where we first examine the computational speed of our method (IV A, before testing its accuracy on small and large molecules (IV B 1, IV B 2). Finally, we showcase our analytical ASC approximation on a presently relevant biomolecular complex: that of the human ACE2 receptor and SARS-CoV-2 spike glycoprotein (IV C).

## II. METHODS

### A. Structures

For testing, we utilize a set of 173 neutral small molecules from version 0.52 of FreeSolv database<sup>78,79</sup>. The original set of nearly 600 molecules was narrowed down to include only those molecules containing hydrogen, oxygen, nitrogen, and carbon atoms. The small molecules under consideration are all rigid - having small conformational variability as seen in molecular dynamic (MD) simulations<sup>80</sup>. The choice of rigid molecules allows us to focus on the physics of solvation, while mitigating the uncertainty related to conformational sampling. *ambpdb*<sup>81</sup> was used to generate PQR format files from AMBER format coordinate and topology files<sup>78</sup>. Additionally, two larger biomolecules are used: a 25 bp poly-A B'-form dsDNA<sup>6</sup>; and the hen-egg lysozyme (PDB:2LZT)<sup>82</sup>. We also test our method on a portion of the ACE2/SARS-CoV-2 complex (PDB:6M0J)<sup>83</sup> receptor binding domain (RBD). 6M0J RBD residues were determined through A/E chain contacts within 3.8 Å. In each chain, residues within 1.5 Å of the contacts were also included. H++ server<sup>84</sup> was used to generate protonated PQR format files. PQR format files for small molecules and the SARS-CoV-2 complex, along with RBD contact residue lists, are provided in the accompanying code package, see the abstract.

### B. Dielectric Boundary Representations

Just like the numerical Poisson solvers, ASC-based methods rely on molecular boundary representations<sup>85-87</sup>. These representations of the actual molecular shape are crucial to the accuracy and, to some extent, efficiency of modern implicit solvation models. The question of which definition of the dielectric boundary (DB) is most appropriate, is non-trivial; there is no universal default<sup>88-90</sup>.

Here, our main goal is to assess the accuracy of the new ASC approximation against its primary accuracy metric, the numerical PB. Both methods can utilize whichever DB one considers most appropriate for the given application. Our secondary goal is to compare the new ASC approximation to a fast analytical GB model. These goals dictate the choice of the DB representation chosen here.

Within our ASC method we approximate the solute-solvent interface – the DB – using the solvent excluded surface (SES)<sup>85,91</sup>, with Bondi<sup>92</sup> atomic radii and a water probe of 1.4 Å. This DB is triangulated with the open-source package, NanoShaper<sup>86</sup>. In each relevant test, we match the NanoShaper grid spacing with that used by the numerical PB reference; we use 0.1 Å for small molecules accuracy comparisons, 0.25 Å for fair speed comparisons, and 0.5 Å for large molecule electric field normal comparisons. The two existing reference methods employed in this work, the NBP and GB, sections IIC and IID, use matching dielectric boundaries based on the same set of Bondi radii with 1.4 Å water probe radius (unless otherwise specified), for consistency.

### C. Numerical Poisson-Boltzmann Reference

For numerical Poisson-Boltzmann (NPB) reference calculations, we use the Macroscopic Electrostatics with Atomic Detail (MEAD) package<sup>93</sup>. MEAD is a volumetric, finite-difference solver that can compute potential maps and hydration energies, utilizing an SES DB representation. The package was chosen primarily because it interfaces well with the visualization and analysis utility GEM<sup>36</sup> used, here to process the NPB-generated potential maps. Using GEM, visualization of the electric field around the solute can be achieved at any given distance from the DB. We have verified convergence<sup>23</sup> of MEAD-generated hydration free energies, Figure 1, and found it acceptable for our purposes at fine enough grid resolutions of interest to us in this work. A modern, 2nd order method MIBPB<sup>94</sup> was used as the accuracy reference for MEAD.

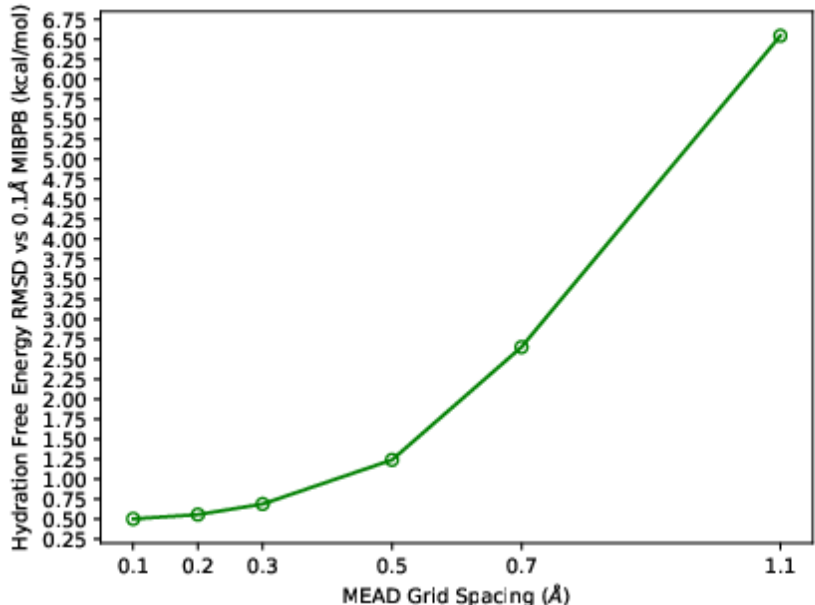


Figure 1: Convergence of hydration free energies computed by MEAD. The convergence is assessed against reference values computed by MIBPB<sup>22</sup>, as RMSD over our small molecule set. MIBPB hydration free energies are computed with a 1.4Å water probe radius at 0.1 Å grid spacing. MEAD hydration free energies are computed with identical parameters, except for the variable grid spacing. MIBPB small molecule electrostatic hydration free energies ranged from -0.05 to -14.37 kcal/mol, with an average magnitude of 6.68 kcal/mol.

Based in part on the convergence analysis, we perform potential-map calculations at a grid spacing of 0.1 Å, and hydration energy calculations at an inner and outer bounding-box grid spacing of 0.1 Å and 0.5 Å, respectively, for small molecule accuracy comparisons. NPB reference solvation energy calculations utilize inner and outer dielectrics of 1 and 80, respectively. The water probe radius is 1.4Å, unless otherwise stated. For fair speed comparisons, we perform potential-map calculations at a grid spacing of 0.25 Å, and hydration energy calculations at a single bounding-box grid spacing of 0.25 Å, considered standard for finite-difference NPB calculations. For larger molecules, we perform potential-map calculations at a grid spacing of 0.5 Å, and hydration energy calculations at an inner and outer bounding-box grid spacing of 0.5 Å and 1.0 Å, respectively. The total number of NPB grid points was determined by setting a volumetric bounding-box side length slightly larger (+1 Å) than the maximal intra-molecular distance. We numerically approximate the electric

field normal at a point  $\mathbf{r}$  by a two-point stencil:

$$\mathbf{E}_\perp(\mathbf{r}) = -\frac{\partial V}{\partial \vec{n}} \approx \frac{V(\mathbf{r} + h\hat{n}) - V(\mathbf{r} - h\hat{n})}{2h}, \quad (3)$$

where  $\mathbf{r} + h\hat{n}$  and  $\mathbf{r} - h\hat{n}$  are two sampling points distance  $r \pm h$  from the DB along the surface normal  $\hat{n}$ ; see Ref.<sup>36</sup> for additional details of the sampling protocol. Here,  $h$  was chosen to minimize the distance between sampled points, while still being large enough so that the sampled points are distinct. Notice that if  $h$  were too small, the sampling protocol would sample the exact same two points of the cubic lattice used in the NPB reference calculations. The largest possible distance between two such grid points is the diagonal of the cubic grid, which determines the minimum  $h$ . To illustrate this numerical constraint,  $h$  must be larger than  $\sqrt{3}/(0.1)^2 \sim 0.173 \text{ \AA}$  for members of the small molecule dataset, whose potential grids were computed with the NPB reference at a grid spacing of  $0.1 \text{ \AA}$ .

Additionally, to avoid numerical artifacts of the NPB reference near the DB, and mitigate possible effects of minor differences between the internal representations of the SES computed by our NPB reference and NanoShaper, the field is computed a distance  $p > h$  from the DB, Figure 4: doing so ensures that we do not accidentally sample grid points inside the molecule. The need to use a non-zero *projection distance* in the NPB calculations makes it necessary to consider the electric field normal values near the DB as the numerical reference for assessing the accuracy of the analytical ASC, rather than the apparent surface charge itself (which, up to a prefactor, is essentially the normal component of the field right at the DB, see equation 5).

#### D. Generalized-Born Solvation Free Energy Reference

We utilize the IGB5<sup>95</sup> GB model from AMBER package<sup>81</sup>. This model was parameterized against reference NPB hydration free energies calculated based on SES surface, Bondi radii, and  $1.4 \text{ \AA}$  water probe radius.

#### E. Accuracy Metrics Used

We test our ASC approximation, first against the exact PB (EPB, see section III A ) reference, and then against NPB and GB references. Our comparison with the EPB

reference is used directly for the apparent surface charge, employing the two test charge configuration in Figure 2b. Per-vertex electric field normal values are compared against the NPB reference, averaging over each vertex in a given biomolecule, and over each biomolecule in the comparison set. Electrostatic hydration free energies are compared against the NPB and GB references with inner and outer dielectrics  $\epsilon_{in} = 1$  and  $\epsilon_{out} = 80$ , unless otherwise specified. All results will be in  $e/\text{\AA}^2$  for apparent surface charge,  $\text{kcal}/(\text{mol} \cdot e \cdot \text{\AA})$  for electric field normals, and  $\text{kcal}/\text{mol}$  for electrostatic hydration free energies.

## F. Computer Specifications

All computations and visualizations were completed on a commodity desktop computer with an Intel Core i7 (or equivalent) processor, using a maximum of 32 GB of memory.

# III. THEORY AND RESULTS

## A. Preliminaries: Analytical Poisson-Boltzmann Reference

In the context of implicit solvation, the simplest scenario is that of a solute with a sharp, spherical DB, Figure 2a.

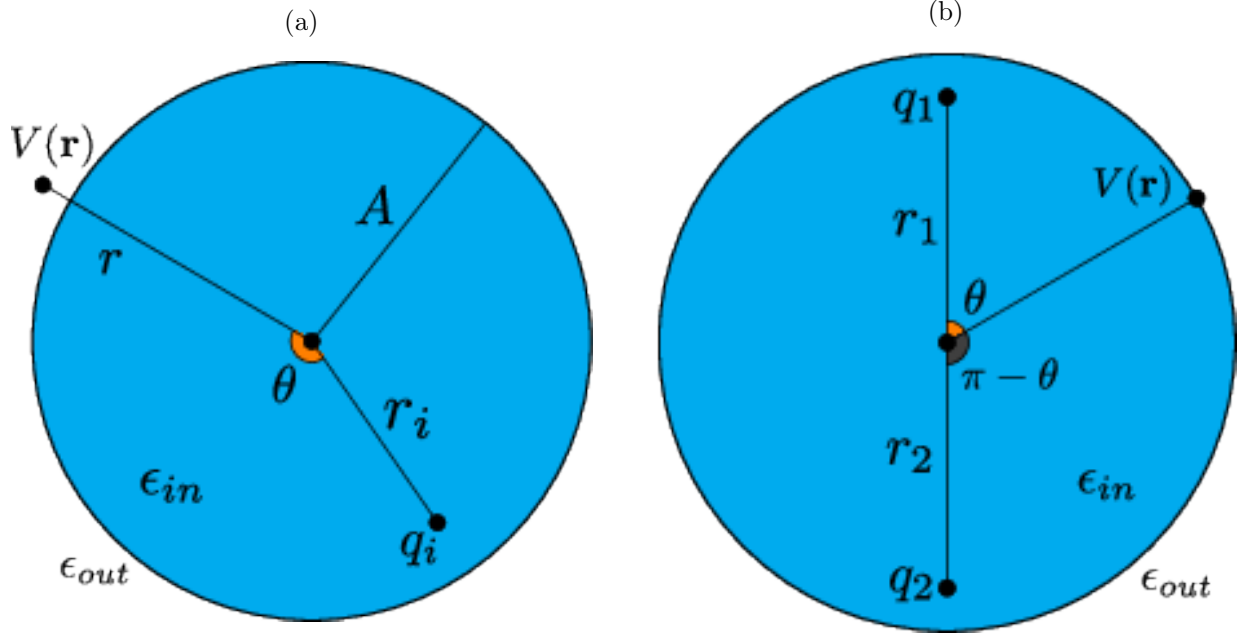


Figure 2: Geometry and charge settings for the Kirkwood multipolar expansion, 2a, and for the two-charge test case, 2b. These notations and geometries are used in equations 4 and 6. In each case, a perfectly spherical, sharp DB is utilized, with  $\epsilon_{in}$  and  $\epsilon_{out}$  denoting inner and outer dielectric constants, respectively. The angle  $\theta$  (resp.  $\pi - \theta$ ) is subtended by the lines connecting the point of observation,  $\mathbf{r}$ , and the charge(s) to the spherical center. In panel 2a, a single point charge,  $q_i$ , is located  $r_i$  away from the center of a spherical boundary with radius  $A$ . In panel 2b, two point charges,  $q_1$  and  $q_2$ , are located on the vertical diameter of the sphere. The charges are of equal distance,  $r_1 = r_2$ , from the spherical center. The electrostatic potential  $V(\mathbf{r})$  is computed at the point of observation  $\mathbf{r}$ .

For such a spherical boundary, as in Figure 2a, Kirkwood<sup>96</sup> gave the exact, analytical solution of equation 1 for the potential  $V_i$  at the DB due to a single charge  $q_i$  inside the boundary. Here, we use the solution valid on or exterior to the spherical DB<sup>97</sup>, without consideration for mobile ions. At  $r = A$ :

$$V_i = -\frac{q_i}{A} \left( \frac{1}{\epsilon_{in}} - \frac{1}{\epsilon_{out}} \right) \sum_{l=0}^{\infty} \left[ \frac{1}{1 + \left( \frac{l}{l+1} \right) \left( \frac{\epsilon_{in}}{\epsilon_{out}} \right)} \right] \left( \frac{r_i}{A} \right)^l P_l(\cos \theta) + \frac{q_i}{A} \left( \frac{1}{\epsilon_{in}} \right) \sum_{l=0}^{\infty} \left( \frac{r_i}{A} \right)^l P_l(\cos \theta). \quad (4)$$

The apparent surface charge  $\sigma$  is related to the normal component of the electric field

$\mathbf{E}_\perp = \left(\frac{\partial V}{\partial \vec{n}}\right)_{out}$  at (just outside) the boundary via:<sup>24,25</sup>

$$\sigma = \frac{1}{4\pi} \left( \frac{\epsilon_{out}}{\epsilon_{in}} - 1 \right) \left( \frac{\partial V}{\partial \vec{n}} \right)_{out}. \quad (5)$$

From this, and equation 4, we obtain an *exact*, analytical expression for the apparent surface charge on the spherical DB:

$$(6) \quad \sigma_{KW} = \sum_i \frac{q_i}{4\pi} \left( \frac{1}{\epsilon_{in}} - \frac{1}{\epsilon_{out}} \right) \left[ \sum_{l=0}^{\infty} \left[ \frac{1}{1 + \left(\frac{l}{l+1}\right) \left(\frac{\epsilon_{in}}{\epsilon_{out}}\right)} \right] (l+1) \left( \frac{r_i^l}{A^{l+2}} \right) P_l(\cos \theta) \right. \\ \left. - \left( \frac{1}{\epsilon_{in}} \right) \sum_{l=0}^{\infty} (l+1) \left( \frac{r_i^l}{A^{l+2}} \right) P_l(\cos \theta) \right],$$

where the summation is over all of the enclosed charges. Equation 6 will provide a key check for our analytical ASC approximation.

### 1. *Convergence Analysis of $\sigma_{KW}$*

The presence of the indexing term,  $(l+1)$ , is notable in its effects on the convergence characteristics of equation 6, by increasing the number of terms necessary to obtain a converged, accurate reference. As the ratio  $r_i/A$  approaches 1 - that is, as the charge approaches the DB - slow convergence of the approximate solution manifests itself.



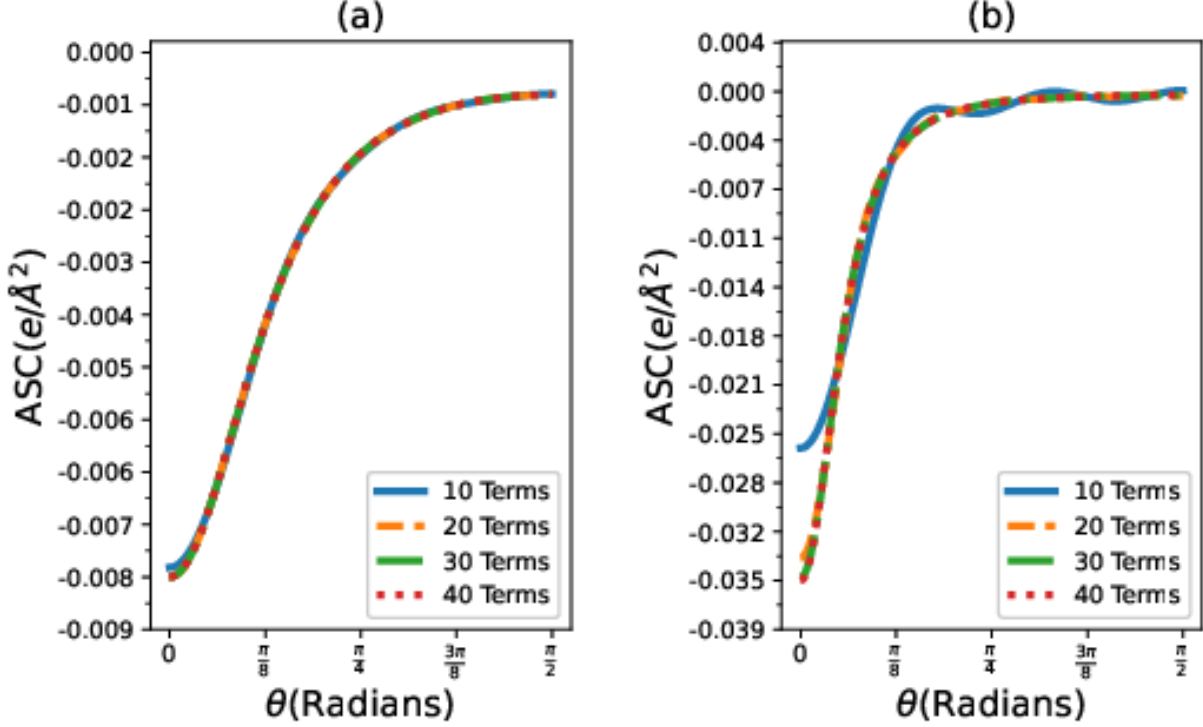


Figure 3: The apparent surface charge (ASC, per unit area) computed using the truncated, infinite series analytical solution of the Poisson problem on a sphere, equation 6. The convergence tests are conducted on the dual-positive test case, Figure 2b. The ASC is sampled at the spherical boundary  $A = 10 \text{ \AA}$  away from the center an angle  $\theta$  from  $q_1$ . Panel (a)  $r_1 = r_2 = 6 \text{ \AA}$ ; (b)  $r_1 = r_2 = 8 \text{ \AA}$ ; see Figure 2b. Partial sums of the infinite series solution, equation 6, with  $M = 10, 20, 30, 40$  terms are examined. The truncated sums are shown with blue, orange, green, and red lines, respectively.

In Panel (b) of Figure 3, we see that, even for  $\frac{r_i}{A} = 0.8$ , it is possible to achieve both qualitatively and quantitatively reasonable results. The analytical reference appears well-converged, Figure 3, for our purposes, at  $M = 30$  terms. Hence, we numerically approximate equation 6 by truncating to the first  $M = 30$  terms, calling the resulting expression the *essentially exact Poisson-Boltzmann (EPB) reference*, which we use further in this work.

## B. Main Result: Analytical Apparent Surface Charge

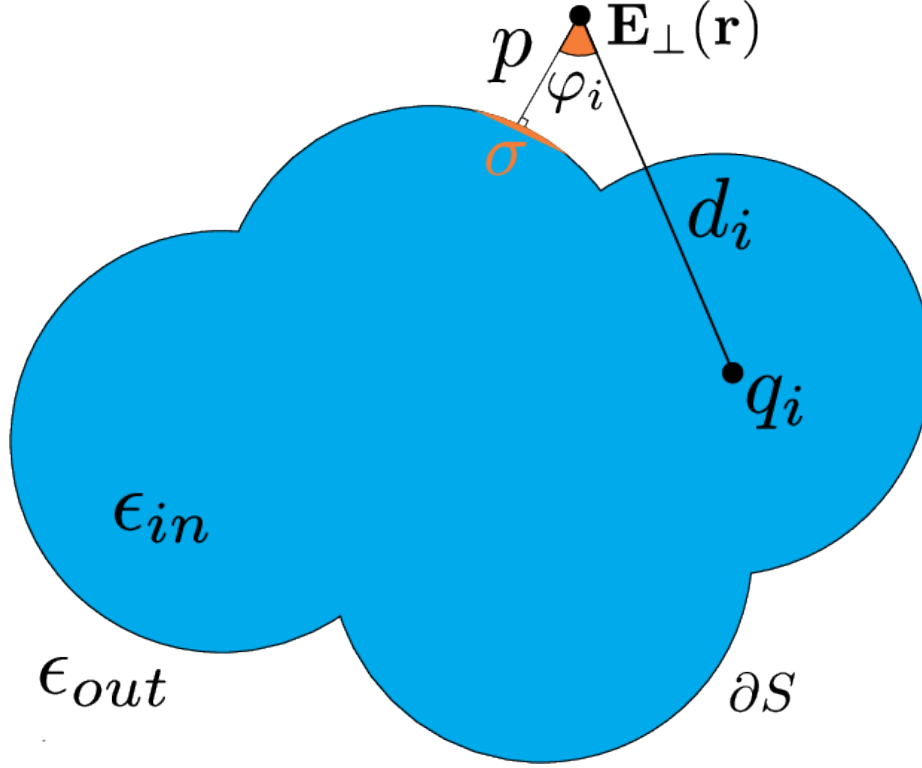


Figure 4: The two dielectric problem for an arbitrary molecule  $S$  with smooth boundary  $\partial S$ . The boundary separates the inner (blue) and outer (white) dielectric regions, with constants  $\epsilon_{in}$  and  $\epsilon_{out}$ , respectively. For a non-spherical DB, the distance  $r$  from the spherical center, Figure 2a, to the sampling point  $\mathbf{r}$  is replaced with the generalized expression  $r = A + p$ . Here,  $A$  is the so-called *electrostatic size* of  $S$ , which characterizes the dimension of the molecule<sup>98</sup>, and  $p$  denotes the *projection distance* from  $\mathbf{r}$  to  $\partial S$  along the surface normal,  $\vec{n}$ .  $q_i$  is the source charge under consideration, with  $d_i$  denoting the distance between  $q_i$  and  $\mathbf{r}$ . When  $p > 0$ , the *electric field normal*  $\mathbf{E}_\perp(\mathbf{r})$  of  $S$  at  $\mathbf{r}$  is computed via equation 9. When  $p = 0$ , the ASC,  $\sigma(\mathbf{r})$ , is computed via equation 10.

To derive our ASC approximation, we begin with the previously derived closed-form approximation for the electrostatic potential around (outside) an arbitrary molecular shape<sup>97</sup>,

see Figure 4:

$$V_i \approx \left( \frac{q_i}{\epsilon_{out} \left( 1 + \alpha \left( \frac{\epsilon_{in}}{\epsilon_{out}} \right) \right)} \right) \left[ \frac{(1 + \alpha)}{d_i} - \frac{\alpha \left( 1 - \frac{\epsilon_{in}}{\epsilon_{out}} \right)}{r} \right]. \quad (7)$$

We utilize the polar orthonormal frame,  $e_r = \frac{\partial}{\partial r}$ ;  $e_\theta = \frac{1}{r} \frac{\partial}{\partial \theta}$ , to take its derivative, for use in equation 5. The derivative vanishes in the direction of  $e_\theta$ , yielding:

$$\mathbf{E}_\perp(\mathbf{r}) = -\frac{\partial V_i}{\partial \vec{n}} = -\left[ \frac{\partial V_i}{\partial r} - \cos(\varphi_i) \frac{\partial V_i}{\partial d_i} \right]. \quad (8)$$

Exploiting the geometry in Figure 4, we relate  $\cos(\varphi_i)$  as a dot product of the surface unit normal,  $\hat{n}$ , and the vector from  $\mathbf{E}_\perp(\mathbf{r})$  to  $q_i$ , which we denote  $\vec{d}_i$ :  $\cos(\varphi_i) = (\hat{n} \cdot \vec{d}_i) / d_i$ . Applying equation 7 to 8, and summing over the charge distribution (Figure 4) we arrive at:

$$\mathbf{E}_\perp(\mathbf{r}) = -\left( \frac{1}{\epsilon_{out} \left( 1 + \alpha \left( \frac{\epsilon_{in}}{\epsilon_{out}} \right) \right)} \right) \sum_i q_i \left[ \left( \frac{\alpha \left( 1 - \frac{\epsilon_{in}}{\epsilon_{out}} \right)}{(A + p)^2} \right) - \cos(\varphi_i) \left( \frac{(1 + \alpha)}{d_i^2} \right) \right], \quad (9)$$

where we have made the substitution  $r = A + p$  described in Figure 4. At the dielectric boundary,  $p = 0$ , applying equation 5 to equation 9 gives the following closed-form, analytical approximation for the apparent surface charge:

$$\sigma = -\left( \frac{1}{\epsilon_{in}} - \frac{1}{\epsilon_{out}} \right) \left( \frac{1}{4\pi \left( 1 + \alpha \left( \frac{\epsilon_{in}}{\epsilon_{out}} \right) \right)} \right) \sum_i q_i \left[ \left( \frac{\alpha \left( 1 - \frac{\epsilon_{in}}{\epsilon_{out}} \right)}{A^2} \right) - \cos(\varphi_i) \left( \frac{(1 + \alpha)}{d_i^2} \right) \right]. \quad (10)$$

These two equations are the main analytical result of this work. Equations 7, 9, and 10 rely on approximating the  $\frac{l}{l+1}$  term of equation 4 as  $\frac{l}{l+1} = \text{const} = \alpha$  for  $l > 0$ , which allows the infinite Kirkwood series to be summed without truncation. That approach proves critical to both accuracy and computational efficiency<sup>97</sup> of the closed-form approximations, based on the Kirkwood solution. The value of  $\alpha$  in equation 7 was rigorously derived previously<sup>99</sup> to minimize RMSD to the exact Kirkwood solution for electrostatic potential, equation 4, assuming a random charge distribution inside a perfect sphere. Here we have attempted to re-optimize the value of  $\alpha$  in the context of equation 10, aiming at best agreement with the reference for hydration free energies of our small molecule set. The effort led to only a very minor improvement in accuracy (not shown), so we have decided to retain the original<sup>99</sup>  $\alpha = 0.580127$  for use in our ASC approximation.

### 1. *A Self-Consistency Check*

Arguably the simplest self-consistency check of analytical ASC is that the total surface charge produced by equation 10 should be zero for any of the neutral small molecules making up our main test set:

$$\oint_{\partial S} \sigma d^2s = 0. \tag{11}$$

In the discrete DB case, as the triangulation density is increased, we expect the numerical approximation of the total charge integral, equation 11, to approach zero. Thus, the same simple check automatically tests both the analytical ASC and the DB discretization (triangulation) used. As seen from Figure 5, our ASC implementation follows the expected trend. We stress that the only purpose of this simple test is a “sanity check” of our code implementation; the accuracy of the derived approximation is tested thoroughly below.

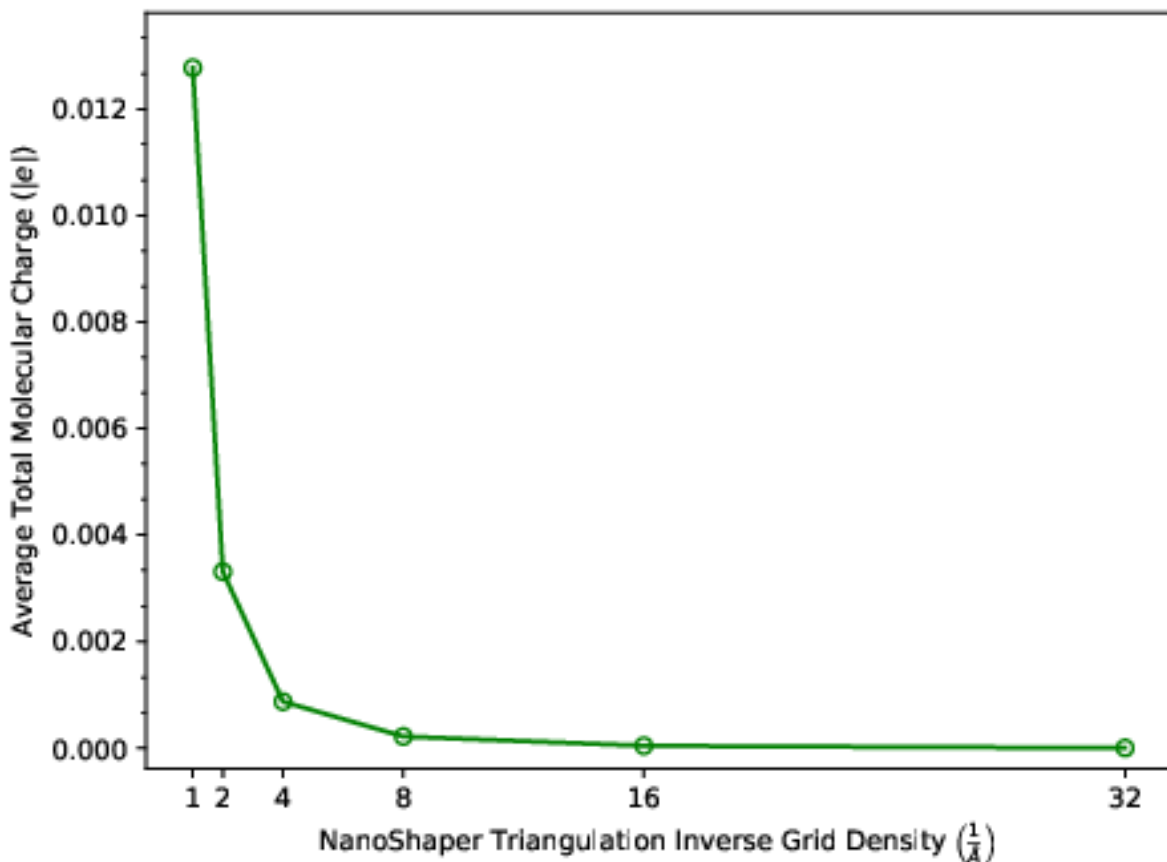


Figure 5: Self-consistency and surface triangulation convergence check of our ASC method. The exact result for the total surface charge is zero; as NanoShaper grid density is increased, the molecular charge estimated via our implementation also tends to zero. An average over the entire set of small neutral molecules is shown. NanoShaper inverse grid spacings are given in  $\text{\AA}^{-1}$ , while average total molecular charges are given in  $|e|$ .

### C. Accuracy against the Analytical PB Reference

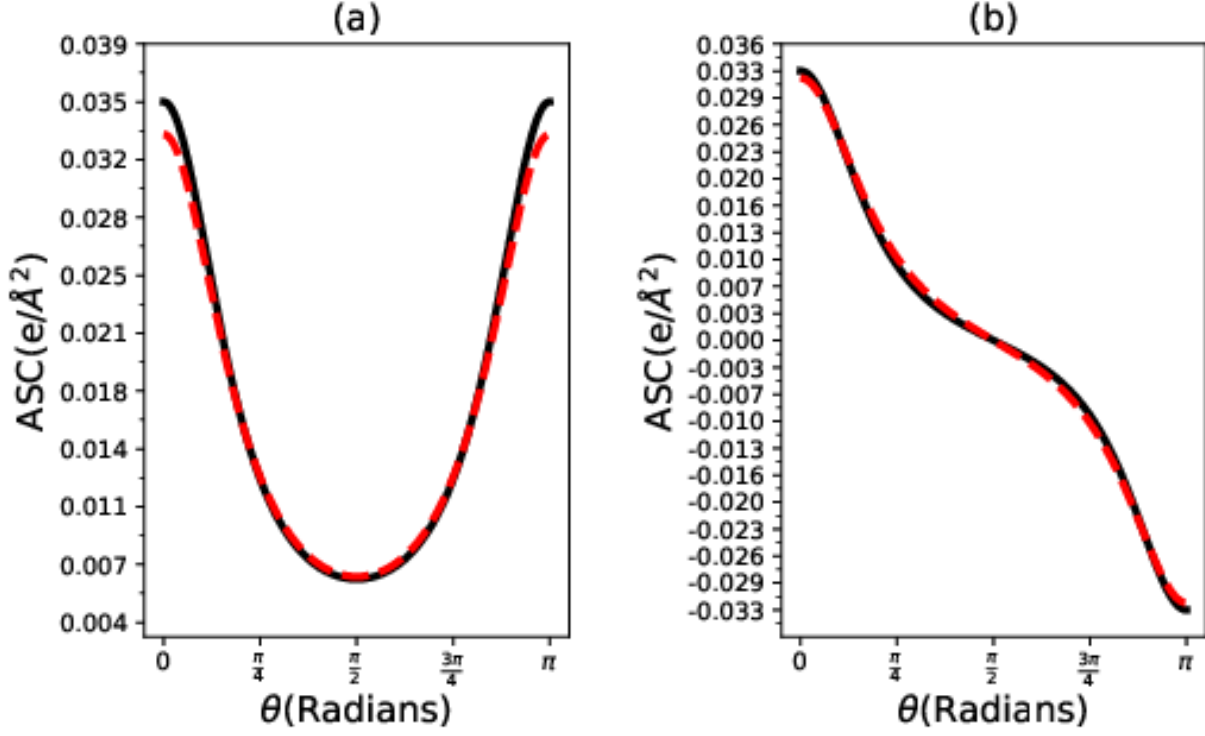


Figure 6: Apparent surface charge of our ASC approximation (dashed red) and the EPB reference (solid black) on the two-charge test distribution, shown in Figure 2b. Panel (a): surface charge due to two point charges,  $1.5 \text{ \AA}$  away from the boundary of a dielectric sphere of radius  $3 \text{ \AA}$ , with  $q_1 = q_2 = -0.65$ . These specific parameters are intended to mimic two oxygen atoms in a small molecule, with respect to the distance between a highly charged “surface” atom and the DB. Panel (b): the same charge distribution as in panel (a), but with  $q_1 = -0.65, q_2 = +0.65$ . Points were sampled from 0 to  $\pi$  in 0.0001 radian steps.

From Figure 6, our approximation matches the essentially exact Kirkwood solution, the truncation of equation 6, quite well on the two-charge test distribution, with only a slight, and expected, drop in accuracy closest to the point charges. For  $\theta \in [0, \pi]$ , an RMSD of  $0.00124e/\text{\AA}^2$  and  $0.00117e/\text{\AA}^2$  was achieved between our ASC approximation and the EPB reference, on the geometries described in panels (a) and (b) of Figure 6, respectively.

## D. Electrostatic Solvation Free Energy with ASC

The apparent surface charge formulation allows us to gain insights into a variety of solvation effects<sup>28,100</sup>, including the estimate of *hydration free energy*, which we will use extensively here to evaluate the accuracy of our new approach against accepted reference. Within the implicit solvation framework<sup>8</sup>, hydration free energy of a molecule is often approximated<sup>101</sup> as the sum of polar (electrostatic) and non-polar components:

$$\Delta G_{solv} = \Delta G_{el} + \Delta G_{np}. \quad (12)$$

Of the two components in equation 12, the *electrostatic solvation free energy*,  $\Delta G_{el}$ , often contributes the most to the total in polar solvents such as water, especially for macromolecules. Highly approximate, yet computationally efficient, ways to estimate the non-polar component,  $\Delta G_{np}$ , are widely used; by comparison,  $\Delta G_{el}$  is relatively expensive to estimate computationally with commonly used numerical methods such as NPB<sup>7</sup>. Here, our focus is  $\Delta G_{el}$ . For a discrete charge density indexed by  $i$  we can compute  $\Delta G_{el}$  as<sup>7</sup>:

$$\Delta G_{el} = \frac{1}{2} \sum_i q_i [V(\mathbf{r}_i) - V(\mathbf{r}_i)_{vac}], \quad (13)$$

where  $V(\mathbf{r}_i)$  and  $V(\mathbf{r}_i)_{vac}$  are the electrostatic potentials due to the given charge distribution in the solvent and in vacuum, respectively, sampled at each point charge  $q_i$  located at  $\mathbf{r}_i$ . In the special case when the inner and outer dielectric constants,  $\epsilon_{in}$  and  $\epsilon_{out}$ , are equal to 1 and 80, respectively, we call  $\Delta G_{el}$  the *electrostatic hydration free energy*. We use equations 2 and 13 to write:

$$\Delta G_{el} = \frac{1}{2} \sum_i q_i \left( \oint_{\partial S} \frac{\sigma(\mathbf{s})}{|\mathbf{r}_i - \mathbf{s}|} d^2s \right). \quad (14)$$

Though equation 14 is valid for any choice of DB, the surface integral is non-trivial to compute. We approximate the surface integral using a specific triangulation of the DB, see section II B. This discrete representation approximates equation 14 as:

$$\Delta G_{el} \approx \left[ \sum_i \sum_T \frac{q_i \sigma_T A_T}{|\mathbf{r}_i - \mathbf{r}_T|} \right], \quad (15)$$

where  $\sigma_T$ ,  $A_T$ , and  $\mathbf{r}_T$  are the apparent surface charge, area, and center of the triangle  $T$  (to express  $\Delta G_{el}$  in kcal/mol, which is often convenient, the equation above is multiplied by 166, while using atomic units of length, Å, and charge,  $|e|$ ). The ASC on  $T$  is found by averaging the ASC at its comprising vertices. The triangular center is simply the centroid of  $T$ , with its area calculated using Heron’s formula:

$$A = \sqrt{d \cdot (d - a) \cdot (d - b) \cdot (d - c)} \quad ; \quad d = \frac{a \cdot b \cdot c}{2}, \quad (16)$$

where  $a$ ,  $b$ , and  $c$  are the side lengths of  $T$ .

## IV. NUMERICAL APPLICATIONS AND RESULTS

### A. Analytical ASC Computational Speed

Here we present general running time descriptions for each tested method, rather than exact time values. In this way, we can differentiate between each method, without worrying about particular optimizations and expert parameter set-ups that can be found across a variety of implementations<sup>102</sup>.

Method	Small Molecules (Average of 16 atoms)	2LZT (1958 atoms)	DNA (1598 atoms)
IGB5(AMBER)	milliseconds	~ a second	~ half a second
Analytical ASC Approximation	~ 100 milliseconds	tens of seconds	~ half a minute
Numerical PB	tens of seconds	minutes	tens of minutes

Table I: Running time expectations for computed electrostatic solvation free energies. Times are given per-molecule (averaged over the entire set in the small molecule case).

In algorithmic time complexity, the three methods we compare in Table I are very different. GB methods, such as the IGB5 reference, scale quadratically in the number of atoms ( $K^2$ ), while our method grows linearly ( $KN$ ) in the number of atoms and surface elements ( $N$ ). Volumetric methods, similar to the NPB reference, scale cubically in the number of grid points per side of a corresponding bounding box, itself a function of grid density and the maximum intra-molecular distance. The impact of these asymptotic time complexities can be clearly seen when we focus on hen-egg lysozyme (2LZT) and double-stranded DNA wall running times. Though the 2LZT structure has about 400 more atoms than the DNA



structure, the intra-molecular width of the DNA structure is almost double that of 2LZT. This means that the DNA structure has both a larger total surface area and requires a bigger volumetric bounding box; as seen in Table I, we find longer running times for our ASC approximation and the NPB reference for 2LZT as compared to DNA, but not for the IGB5 reference. Hence, this contrasting algorithmic complexity affects computational timings between each model for structures of different size and characteristic. A principal consequence is the following: The best case scenario for the efficiency of our ASC approximation is for structures having many atoms, but a comparatively low surface area; in terms of the derivation of our model, it is coincidental that in three dimensions the shape maximizing total inner “volume” (number of atoms) and minimizing outer surface area is that of a sphere.

Though the efficiency of our analytical ASC implementation is not at the level of the IGB5 reference, it occupies a different niche: its main purpose is the estimation of the ASC and the electric field. It is worth noting that the surface integration required for equation 15 is trivially parallel, since equations 9 and 10 can be computed independent of adjacent surface elements on the DB. This is in addition to the more fundamental parallelism present in equations 9 and 10, due to the independence of per-charge contributions to the electric field and ASC, respectively. Improvements in the efficiency of our implementation would greatly improve performance as surface resolution is increased, or in “worst-case” scenarios such as those seen in the DNA fragment, Table I.

## B. Analytical ASC Accuracy with respect to the NPB Reference

### 1. *Small Molecules*

*a. Qualitative Visualizations* We first examine how our ASC approximation compares to the NPB reference *qualitatively*. Here, our motivation is the well recognized utility<sup>6,9,83</sup> of visualizing electrostatic characteristics of molecules, including mapping them onto a molecular surface. Our main metric, in this section, is qualitative similarity, or lack thereof, between visualizations produced by our analytical ASC method and the NPB reference.

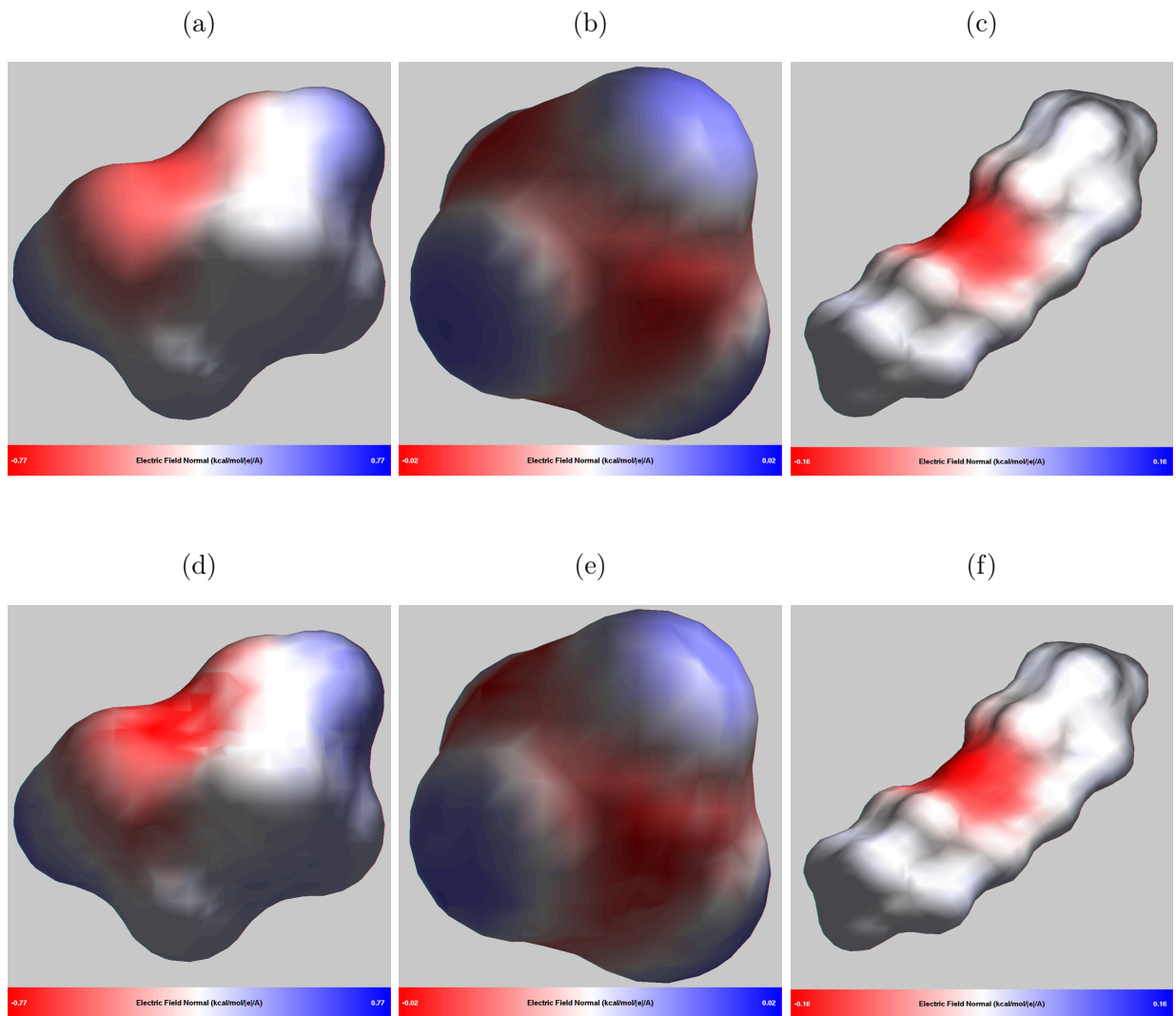


Figure 7: Electric field normals computed on a selection of small molecules by our ASC approximation (top row) and the NPB reference (bottom row), with visualization by GEM<sup>36</sup>. From left to right, the three molecules shown (chosen to represent various shapes) are 1,2-ethanediol (7a, 7d), methane (7b, 7e), and 1-Butoxybutane (7c, 7f). All calculations are made 0.7 Å from the DB, with a water probe radius of 1.4 Å. Our ASC approximation and the NPB reference use a 0.1 Å triangulation density/grid spacing. The color range for the analytical ASC and the NPB reference is the same for each vertical pair of panels.

Figure 7 exemplifies the qualitative match between our method and the NPB reference on a subset of the small molecule data set. Apart from very small irregularities, attributable

to the discrete sampling of the NPB potential map, the electric field normals computed with our ASC approximation are, visually, almost indistinguishable from those computed with the NPB reference.

The near quantitative agreement between the analytical ASC and the NPB reference, Figure 7 is nontrivial, and goes beyond the visual match of the “reds” and the “blues” with the NPB reference. Notice that, when  $\alpha$  is set to 0 in equations 7 and 9, the analytical ASC reduces to the so-called *Coulomb Field Approximation* (CFA), which is often used, and can be considered a Null model here.

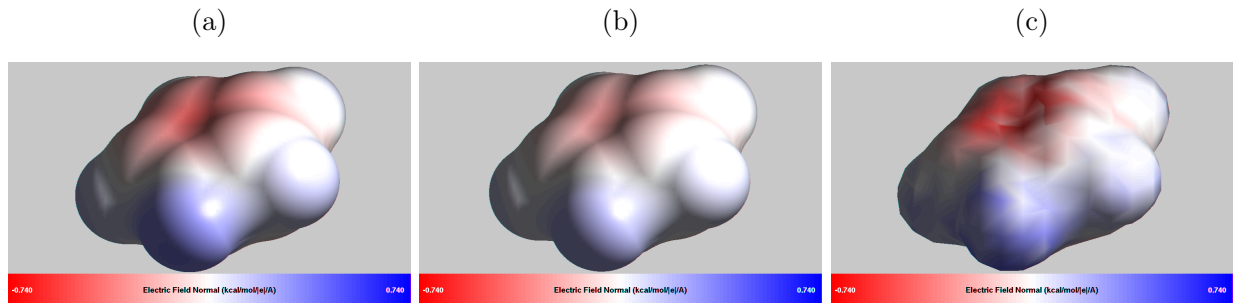


Figure 8: Electric field normals computed via our Analytical ASC method (Panel 8a), the *Coulomb Field Approximation* (CFA) (Panel 8b), and the NPB reference (Panel 8c) on a member of our small molecule data set, pyrrole. While both the analytical ASC and the CFA identify the positive and negative surface charge patches, the CFA underestimates their intensity significantly. Between the analytical ASC method and the CFA, minimum, maximum, and average electric field normals on the DB are  $-0.441, 0.314$ , and  $-0.030$  kcal/(mol  $\cdot e \cdot \text{\AA}$ ) and  $-0.281, 0.200$ , and  $-0.019$  kcal/(mol  $\cdot e \cdot \text{\AA}$ ), respectively. The color range used to visualize the field is the same in all the panels.

Figure 8 clearly indicates the decreased magnitude of CFA-generated electric field normals, when compared to our ASC approximation; on average, the CFA produces an electric field that is approximately 36% weaker than our analytical ASC method, which reproduces the NPB reference closely. The significant deviation of the CFA surface charge from the reference translates into its poor accuracy in estimation of the hydration free energy, Figure 9 below.

*b. Quantitative assessment of ASC accuracy* Next, we examine how our ASC approximation compares *quantitatively* to the NPB reference. Though electric field normals (or linearly related surface charges) are not the most intuitive accuracy metrics, these quantities are those that our method *directly* computes, and so a direct comparison with the NPB is in order. In section IV B 3, we discuss a physical interpretation of the deviation of these quantities from the reference. Relative to the NPB reference, our ASC approximation achieves an average RMSD and absolute difference of 0.14 and 0.11 kcal/(mol  $\cdot$  e  $\cdot$  Å) on calculated electric field normal values, respectively.

*c. Electrostatic Solvation Free Energy* Relative to direct comparisons of molecular ASC, or its proxy, the normal electric field, tests featuring the calculation of electrostatic solvation free energies are valuable in the sense that they provide an intuitive accuracy metric, directly relevant to experiment. Here, IGB5<sup>95</sup> is an example of what can be expected from a very fast GB model on small molecule data sets<sup>103,104</sup>, in terms of accuracy and running time. We test how our ASC approximation and the IGB5 method compares to calculation of electrostatic solvation free energies by the NPB reference.

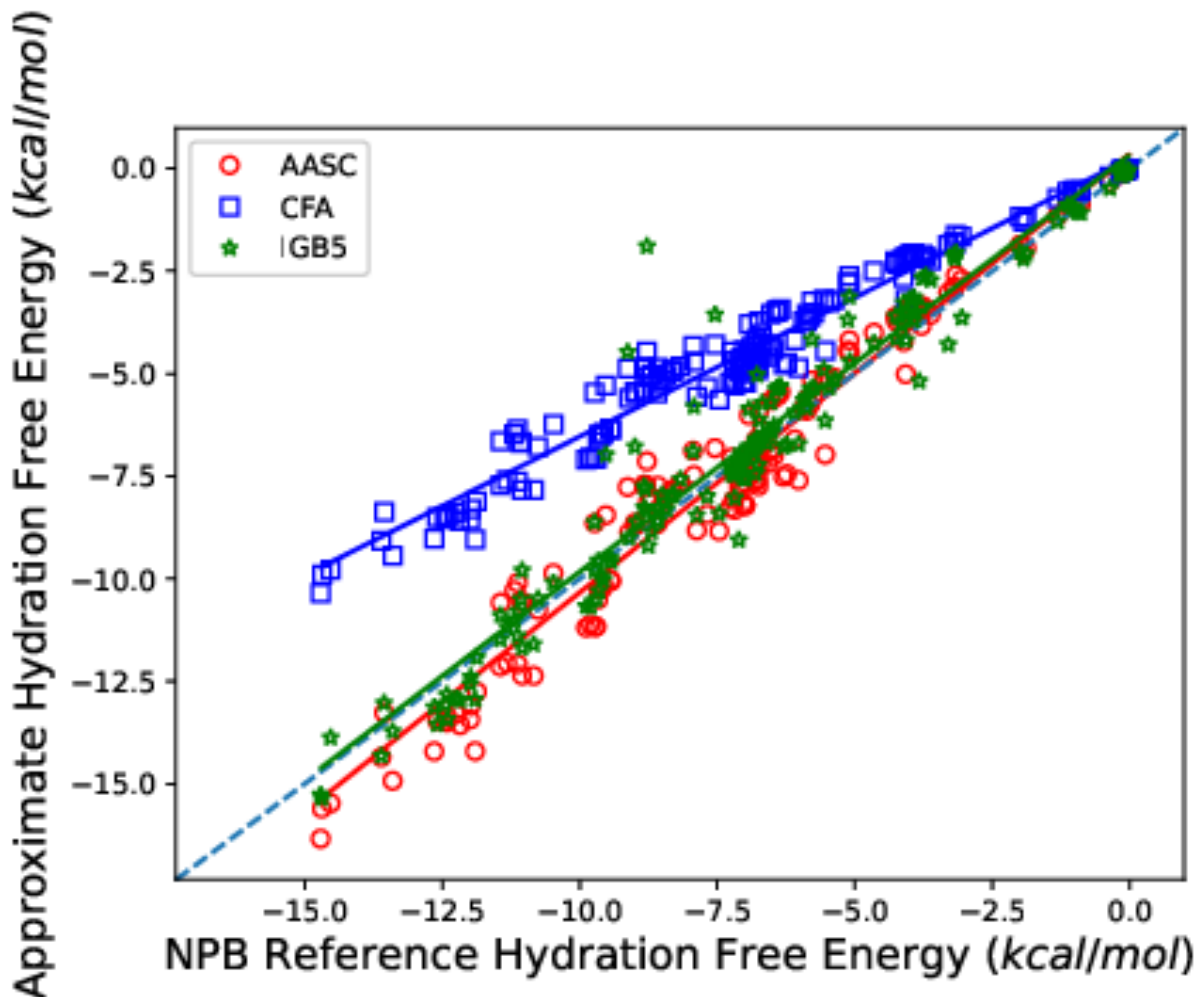


Figure 9: Analytical ASC (red circles), the GB (green stars) and CFA (blue squares) hydration free energies of rigid small molecules relative to the NPB reference values. Linear regression lines are plotted using colors corresponding to the representative data points. The dotted blue line represents the perfect match between an approximation and the NPB reference.  $R^2$  values for IGB5, our analytical approximation, and the CFA are 0.932, 0.961, and 0.777, respectively. Hydration free energies are shown in kcal/mol.

Using the analytical ASC approximation given in equation 10,  $\Delta G_{el}$  is computed through the use of equation 14. Our ASC approximation yielded a 0.77 kcal/mol RMSD to NPB reference hydration free energies, while the GB reference showed 0.98 kcal/mol on the same metric. Not surprisingly, the CFA accuracy is much worse, 2.73 kcal/mol away from the NPB reference. In this comparison, NPB reference small molecule electrostatic hydration free energies ranged from -0.02 to -14.71 kcal/mol.

From our findings above, our ASC approximation has an approximately 20% reduced RMSD to NPB reference hydration free energies than the IGB5 reference. This accuracy gain is encouraging, particularly from the perspective of design: GB models are designed to analytically approximate the electrostatic solvation free energy obtained from solving the Poisson equation. That our model can estimate solvation energies more accurately than a widely used GB model suggests that the approximation of the ASC and electric field normals by the model is reasonably accurate to be considered for practical applications. Additionally, the results achieved above give another encouraging conclusion, with respect to running times efficiencies. To achieve a deviation from the NPB reference of just slightly above  $kT$ , we do not require an overly fine triangulation density for the analytical ASC. When the grid resolution is set to what is used in the timing section above (Table I), RMSD against the NPB reference, differs only in non-significant digits. Thus, our analytical ASC can achieve a very similar accuracy, without incurring a heavy 1-2 order of magnitude time penalty, as seen with the NPB reference at this fine grid resolution.

## 2. *Proteins and DNA*

In analyzing the performance of our model on structures of increased size and complexity, we examine a fragment of double-stranded DNA and the hen-egg lysozyme. Structures of this type - with regions of the DB having deep, negative curvature "pockets" - present some of the toughest tests for our model, due to certain theoretical considerations we touch on below.

### *a. Qualitative Visualizations*

**Double-Stranded DNA.** First, we examine our analytical approximation on a double-stranded DNA fragment.

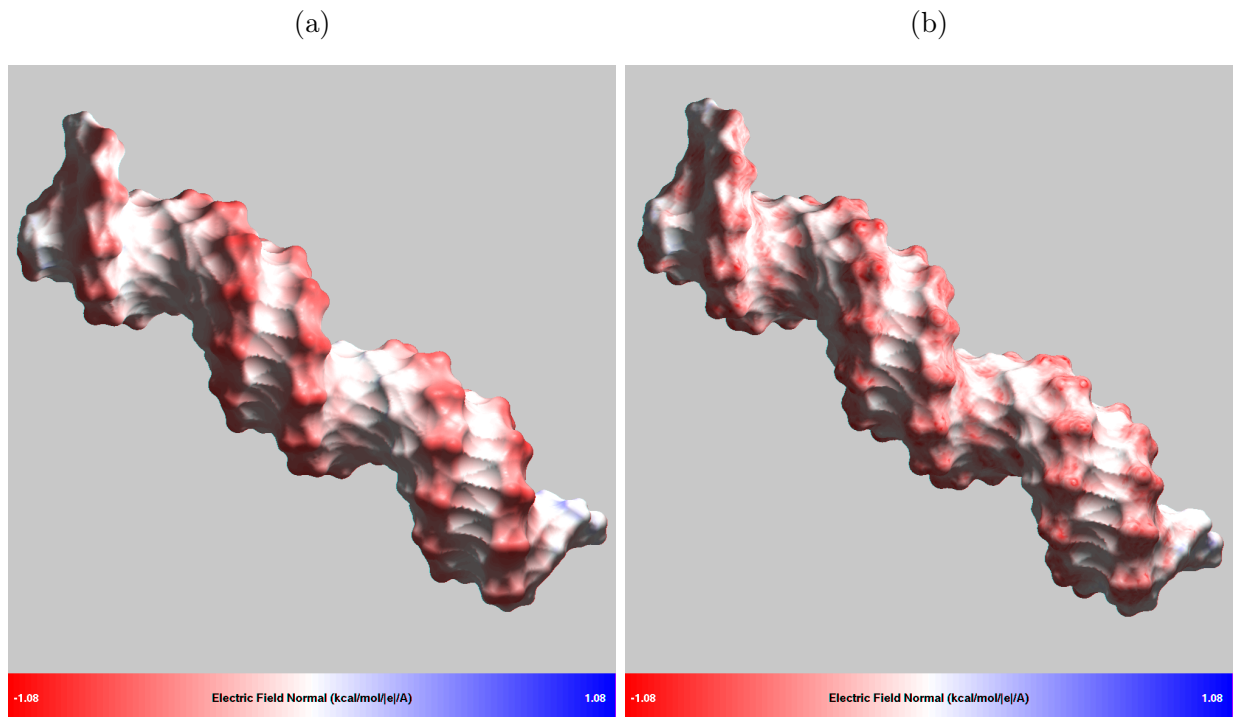


Figure 10: Electric field normals computed on the double-stranded DNA snapshot by our ASC approximation, Panel 10a, and the NPB reference, Panel 10b, with visualization by GEM<sup>36</sup>. The field is estimated 1.5 Å from the DB, obtained with the water probe of radius of 2 Å. The larger probe radius is used here to achieve a better visualization of negative curvature regions. Our ASC approximation and the NPB reference use a 0.5 Å triangulation density/grid spacing.

Qualitatively, Figure 10 shows that our analytical approximation reproduces the NPB reference quite well, although some discrepancies are clearly seen in the grooves, that is in the regions of negative curvature, see a discussion below.

**Triclinic Hen Egg White Lysozyme** Next, we compare our analytical ASC to the NPB reference on the triclinic hen egg white lysozyme.

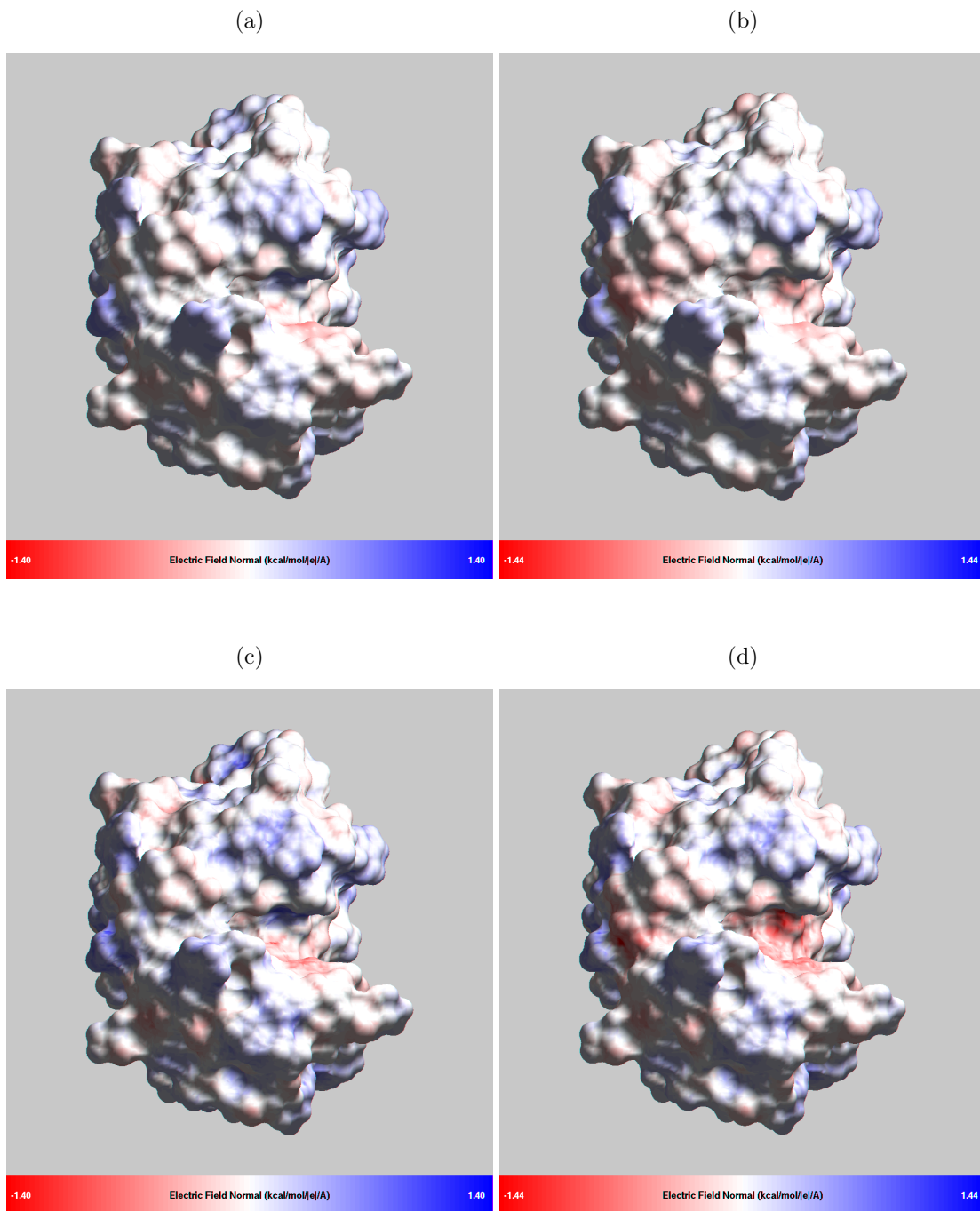


Figure 11: Electric field normals computed on the hen-egg lysozyme by our ASC approximation (top row) and the NPB reference (bottom row), with visualization by GEM<sup>36</sup>. Panels 11a and 11c: the structure at pH 4.5. Panels 11b and 11d: the structure at pH 6.5. All calculations are made 1.5 Å from the DB, with a water probe radius of 2 Å. The larger probe radius is used to achieve a better visualization of negative curvature regions. Our ASC approximation and the NPB reference use a 0.5 Å triangulation density/grid spacing.



We see in Figure 11 that our analytical approximation accurately reproduces the NPB reference, outside of the hen-egg lysozyme’s binding cleft. Within the binding cleft, quantitative deviations in electric field normal magnitudes from the NPB reference become apparent, though our approximation still produces a qualitatively reasonable picture. Our approximation (Figure 11a  $\rightarrow$  11b) qualitatively reproduces the reference (Figure 11c  $\rightarrow$  11d), in visualizing the substantial electrostatic effect of Asp 52 and Glu 35 in the enzymatic pocket, as well as the corresponding changes due to the change in the charge states of these two residues under mildly acidic conditions (pH 4.5). Hence, both the NPB reference and our model are able to visualize the behavior of Asp 52 and Glu 35, under pH change<sup>105–107</sup>.

*b. Quantitative Comparisons* With qualitative tests complete, we finish the analysis with a quantitative comparison between our analytical approximation and the NPB reference.

	Double-Stranded DNA	2LZT pH 4.5	2LZT pH 6.5
<b>Absolute Difference</b>	0.27	0.15	0.15
<b>Average RMSD</b>	0.37	0.19	0.20

Table II: Electric field normal comparisons between our analytical approximation and the NPB reference, on double-stranded DNA and the protonated/un-protonated hen-egg lysozyme. All values are in kcal/(mol  $\cdot e \cdot \text{\AA}$ ).

As expected, quantitative performance deficiencies exist for larger molecules with prominent regions of negative curvature. Although the double-stranded DNA and hen-egg lysozyme have similar numbers of atoms, average RMSD values in Table II are, relatively, inconsistent. On the double-stranded DNA snapshot ( $\sim 1600$  atoms), the average RMSD against the NPB reference is about 2.6 times larger than on small molecules (section IV B 1 b, Table II). Comparatively, the average RMSD of the hen-egg lysozyme ( $\sim 2000$  atoms) is only about 1.4 times larger than on small molecules. On hydration free energies, relative errors between our analytical approximation and the NPB reference are quite small on the DNA snapshot,  $\sim 4\%$ , but more than double,  $\sim 12\%$ , on the hen-egg lysozyme. These findings might have to do with the DNA’s proportion of negative curvature regions with respect to the whole.

### 3. Discussion

*a. Surface Charge Distribution and Electrostatic Solvation Free Energy* To put the results of section IV B 1 b and Table II in a better context, it may be helpful to consider a hypothetical situation. Suppose a biomolecule of interest has a constant electric field strength near its dielectric boundary. When compared to the reference, there is, on average, a  $\sim 0.4$  kcal/(mol  $\cdot e \cdot \text{\AA}$ ) RMSD error in the electric field normal values. If a unit electric charge was moved 1  $\text{\AA}$  away from the biomolecular boundary, along the surface normal, the error in the total work done by the electric field would be less than  $\sim 0.4$  kcal/mol - small when compared to the “gold-standard” 1 kcal/mol difference against reference. Several caveats are due here. First, the estimate is based on the RMS error; it is possible that the errors are larger in some spots near the DB. That concern is mitigated to an extent by the fact that the electric field strength is inversely related to the square of distance from the surface, and would, in reality, decrease away from the surface, making any discrepancy with the reference smaller. Second, this test is free from the danger of a specific error cancellation that may affect the commonly used error assessment based on solvation free energies. As the history of the GB model development demonstrates<sup>42</sup>, very large errors in individual contributions may cancel out to produce seemingly accurate total solvation energies.

*b. Structural Considerations* A notable feature, seen prominently in both the double-stranded DNA snapshot and the hen-egg lysozyme, but not generally in small molecules, is the presence of distinct, and fairly deep, negative curvature pockets on the DB. Our analytical ASC model is derived from an exact solution of the Poisson problem on a spherical DB (Figure 2a), having positive curvature throughout. Negative curvature regions, such as the main groove in Figure 10 and the binding cleft in Figure 11, do not occur on a sphere; this is where our model is not expected to perform well. A resulting loss in performance had been noted previously<sup>36</sup> for the approximate electrostatic potential (equation 7). It is therefore surprising that a qualitative agreement with the NPB reference is still seen, even in these regions. More shallow negative curvature regions are also present in the small molecules, Figure 7, but apparently these do not present a significant challenge to the new model.

Confounding this effect, deep negative curvature regions on the DB can restrict water molecule conformational freedom, making nearby solvent behave less similar to that of the

bulk<sup>108,109</sup>. It has been shown that regions of this type can significantly modify interactions between small molecule inhibitors and their target proteins<sup>110</sup>, prompting investigations related to their identification<sup>111,112</sup>. In our context, this change in the behavior of water bulk has negative implications on the performance of our model, but the same is true for the NPB reference, which is also based on the continuum solvent. Because both of these models are expected to deviate from the correct physical behavior within these regions of negative curvature, we argue that a qualitative agreement with the NPB reference may be acceptable here, in place of a strong quantitative agreement.

*c. Computational Considerations* Though not implemented in this work, one very important consequence of our analytical approach to the ASC confers a key additional theoretical benefit – the trivially parallel nature of our solution. Equation 10 is computed over our *discrete* DB representation, and is totally independent from surrounding surface elements. Coupled with a similarly parallelizable expression for the computation of electrostatic solvation free energy, equation 15, our method holds significant potential for the computationally efficient ASC treatment of large biomolecules.

### C. Testing on a Large Biomolecule

For a real-world application, we examine our approximation on a much larger ( $\sim 6500$  atom) complex, with important relevance today - the ACE2/SARS-CoV-2 complex (PDB ID:6M0J).

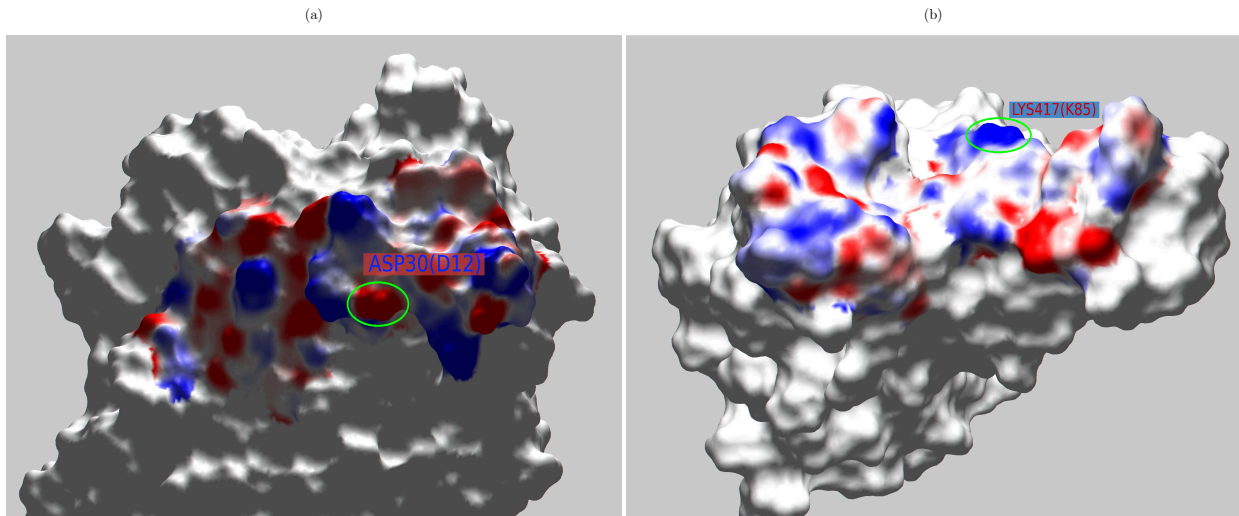


Figure 12: Apparent surface charge computed on the receptor binding domain (RBD) of ACE2 receptor/SARS-CoV-2 spike glycoprotein complex, with visualization by GEM<sup>36</sup>. The range of the ASC values is  $\pm 0.008 e/\text{\AA}^2$ , corresponding to the red-blue color map. White area – the majority of the molecular surface outside of the RBD – is excluded from the calculation, which reduces the computational time significantly. To mimic the color convention used in Figure 1 (B) of Wang et al<sup>83</sup>, the sign of equation 10 is reversed for this calculation, that is the negative of the  $\sigma$  is shown. Figures 12a and 12b show the ACE2 receptor and SARS-CoV-2 spike glycoprotein RBDs, respectively. All calculations are made 0.7  $\text{\AA}$  from the DB with a water probe radius of 2  $\text{\AA}$ . A NanoShaper triangulation density of 0.5  $\text{\AA}$  is used.

Recently, a comparison has been made between SARS-CoV and SARS-CoV-2, examining various mutations and their effects on respective binding strengths with the ACE2 agonist<sup>83</sup>. The focus of Figure 12 is on, what Wang<sup>83</sup> terms, the “CR2” receptor binding domain; the visualized ASC shows how our approximation reproduces the electrostatic complementarity of surfaces charges between two residues, ASP30 (D12), Figure 12a, and LYS 417 (K85), Figure 12b, thought to contribute to the formation of a salt bridge. This salt bridge improves both stability and binding strength between the ACE2 receptor and SARS-CoV-2 spike protein, when compared to the SARS-CoV spike protein.

These large-scale visualizations of the ASC (or of the normal component of the electric field) has already been shown useful<sup>113</sup>; our analytical approximation might be a useful tool in understanding complex protein-protein interactions at a atomistic scale, including

SARS-CoV-2 mutants of concern<sup>114</sup>, especially in high throughput studies. Our method can potentially be useful in this area due to its targeted, *source-based* approach to computation of ASC, where only a small portion the entire DB, and hence a small subset of the surface elements, is included in the computation, as demonstrated in Figure 12. As a result, the compute time is reduced dramatically, see the discussion on time complexity above.

## V. CONCLUSION

In this work, we have derived a closed-form, *analytical* approximation for biomolecular apparent surface charge (ASC), and the normal component of the electric field outside the molecule. To the best of our knowledge, this is the first such fully analytical approximation. The approximation is constructed to closely reproduce the exact infinite series solution for a perfect spherical boundary; more importantly, the approximation yields a reasonably close agreement with the standard numerical PB for realistic molecular structures. Specifically, quantitative reproduction of results from the standard numerical PB reference is achieved on most of the tested molecules, except within prominent regions of negative curvature, where the new approximation is still qualitatively correct. Comparisons with a popular fast GB model in AMBER (IGB5) shows that our method is more accurate in reproducing the hydration free energy, albeit at higher computational expense, which may be expected of proof-of-concept code package that is not highly optimized. At the same time, standard numerical PB is still 1-2 orders of magnitude slower than the proposed approximation, which puts it "in-between" fast analytical GB and numerical PB. We stress that solvation free energy estimates are used here as a common and convenient accuracy metric, and is not where we believe the potential benefits of the proposed analytical ASC may be. These potential benefits stem from the unique features of the method.

There are at least two features of the new approximation absent from the GB: the ability to estimate the apparent surface charge (and, hence, the potential everywhere); and the ability to estimate the normal component of the electric field. Another noteworthy feature of the approach sets it apart from other existing approximations that can estimate ASC, including those aimed at computing ASC directly – the fact that the new approximation is "source-based". This means that the normal electric field and the ASC can be estimated at any individual point or surface patch, without the need for self-consistent computation

over the entire surface or volume. This feature is in contrast to “field-based” methods such as numerical solutions of the Poisson equation or DPCM. As an illustration, we showed that the “source-based” feature of our ASC approximation allows a rapid examination of the ACE2/SARS-CoV-2 RBD electrostatics, reproducing conditions posited to contribute to the spike protein’s high binding strength.

An area which, in our view, can benefit the most from the proposed analytical ASC is the development of new implicit solvation methods that require fast estimates of local polarization charges or/and fields. We also believe the new approach may have the potential to compete with existing ASC-based approaches in QM applications, especially where computational efficiency is key; further extensive testing and analysis beyond the scope of the proof-of-concept work will be necessary to explore the potential of the method in this area.

As it stands, the proposed method has several limitations. First, it does not yet include salt effects explicitly. However, in the future, it should be relatively easy to add into the model salt dependence at the Debye-Huckel level, following an approach outlined in Ref.<sup>97</sup>. Another limitation of the model is its qualitative nature in the regions of high negative curvature, at least relative to the standard NPB reference. Overcoming this specific limitation will require a significant extension of the underlying theory, and extensive testing on biomolecular structures.

A careful and detailed comparison of our proof-of-concept approximation within the broader category of existing, optimized implementations ASC methods has not been performed, and is warranted in the future; nonetheless, promising results so far have pointed to the potential of our approach in forming the basis of novel implicit models of solvation.

## VI. ACKNOWLEDGMENTS

We would like to thank Nitin Passa for his contributions to the numerical ideas behind this application of ASC. In addition, we appreciate the help of Dr. Igor Tolokh for supplying the double-stranded DNA snapshot, and Dr. Andrew Fenley for his useful comments and suggestions.

## VII. AUTHOR DECLARATIONS

A.V.O. reports support from the NIH, grant R21GM131228.

### A. Conflict of Interest

The authors have no conflicts to disclose.

## VIII. DATA AVAILABILITY

The data that support the findings of this study are available from the corresponding author upon reasonable request.

## REFERENCES

- <sup>1</sup>H.-X. Zhou and X. Pang, Chemical Reviews **118**, 1691 (2018).
- <sup>2</sup>S. A. Adcock and J. A. McCammon, Chemical reviews **106**, 1589 (2006).
- <sup>3</sup>M. Karplus and J. A. McCammon, Nature Structural Biology **9**, 646 (2002).
- <sup>4</sup>E. P. Raman and A. D. MacKerell, Journal of the American Chemical Society **137**, 2608 (2015).
- <sup>5</sup>R. E. Amaro and A. J. Mulholland, Journal of Chemical Information and Modeling **60**, 2653 (2020).
- <sup>6</sup>I. S. Tolokh et al., Nucleic Acids Research **42**, 10823 (2014).
- <sup>7</sup>A. V. Onufriev and S. Izadi, Wiley Interdisciplinary Reviews: Computational Molecular Science **8**, e1347 (2017).
- <sup>8</sup>C. J. Cramer and D. G. Truhlar, Chemical Reviews **99**, 2161 (1999).
- <sup>9</sup>B. Honig and A. Nicholls, Science (New York, N.Y.) **268**, 1144 (1995).
- <sup>10</sup>P. Beroza and D. A. Case, Methods in Enzymology **295**, 170 (1998).
- <sup>11</sup>J. D. Madura et al., Biological Applications of Electrostatic Calculations and Brownian Dynamics Simulations, in Reviews in Computational Chemistry, pages 229–267, John Wiley & Sons, Ltd, 1994.
- <sup>12</sup>M. K. Gilson, Current Opinion in Structural Biology **5**, 216 (1995).

- <sup>13</sup>M. Scarsi, J. Apostolakis, and A. Caffisch, *The Journal of Physical Chemistry A* **101**, 8098 (1997).
- <sup>14</sup>R. Luo, L. David, and M. K. Gilson, *Journal of Computational Chemistry* **23**, 1244 (2002).
- <sup>15</sup>T. Simonson, *Reports on Progress in Physics* **66**, 737 (2003).
- <sup>16</sup>N. A. Baker, D. Bashford, and D. A. Case, Implicit Solvent Electrostatics in Biomolecular Simulation, in *New Algorithms for Macromolecular Simulation*, edited by B. Leimkuhler et al., *Lecture Notes in Computational Science and Engineering*, pages 263–295, Springer, Berlin, Heidelberg, 2006.
- <sup>17</sup>J. P. Bardhan, *Computational Science & Discovery* **5**, 013001 (2012).
- <sup>18</sup>L. Li, C. Li, Z. Zhang, and E. Alexov, *Journal of Chemical Theory and Computation* **9**, 2126 (2013).
- <sup>19</sup>W. Rocchia, E. Alexov, and B. Honig, *The Journal of Physical Chemistry B* **105**, 6507 (2001).
- <sup>20</sup>A. Nicholls and B. Honig, *Journal of Computational Chemistry* **12**, 435 (1991).
- <sup>21</sup>N. A. Baker, D. Sept, S. Joseph, M. J. Holst, and J. A. McCammon, *Proceedings of the National Academy of Sciences of the United States of America* **98**, 10037 (2001).
- <sup>22</sup>D. Chen, Z. Chen, C. Chen, W. Geng, and G.-W. Wei, *Journal of Computational Chemistry* **32**, 756 (2011).
- <sup>23</sup>D. D. Nguyen, B. Wang, and G.-W. Wei, *Journal of Computational Chemistry* **38**, 941 (2017).
- <sup>24</sup>J. D. Jackson, *Classical Electrodynamics*, Wiley, New York, 3rd ed edition, 1999.
- <sup>25</sup>S. Miertuš, E. Scrocco, and J. Tomasi, *Chemical Physics* **55**, 117 (1981).
- <sup>26</sup>S. Miertus and J. Tomasi, *Chemical Physics* **65**, 239 (1982).
- <sup>27</sup>A. Onufriev, Continuum Electrostatics Solvent Modeling with the Generalized Born Model, in *Modeling Solvent Environments*, chapter 6, pages 127–165, John Wiley & Sons, Ltd, 2010.
- <sup>28</sup>L. Onsager, *Journal of the American Chemical Society* **58**, 1486 (1936).
- <sup>29</sup>J. Barker and R. Watts, *Molecular Physics* **26**, 789 (1973).
- <sup>30</sup>A. Klamt, *The Journal of Physical Chemistry* **99**, 2224 (1995).
- <sup>31</sup>J. Tomasi, B. Mennucci, and R. Cammi, *Chemical Reviews* **105**, 2999 (2005).
- <sup>32</sup>J. M. Herbert, *WIREs Computational Molecular Science* **11**, e1519 (2021).



- <sup>33</sup>T. N. Truong and E. V. Stefanovich, *Chemical Physics Letters* **240**, 253 (1995).
- <sup>34</sup>M. Cossi and V. Barone, *The Journal of Chemical Physics* **109**, 6246 (1998).
- <sup>35</sup>A. Klamt and G. Schüürmann, *Journal of the Chemical Society, Perkin Transactions 2* **1**, 799 (1993).
- <sup>36</sup>J. C. Gordon, A. T. Fenley, and A. Onufriev, *The Journal of Chemical Physics* **129**, 075102 (2008).
- <sup>37</sup>G. Hoijtink, E. De Boer, P. Van der Meij, and W. Weijland, *Recl. Trav. Chim. Pays-Bas* **75**, 487 (1956).
- <sup>38</sup>S. C. Tucker and D. G. Truhlar, *Chem. Phys. Lett.* **157**, 164 (1989).
- <sup>39</sup>D. Qiu, P. Shenkin, F. Hollinger, and W. C. Still, *J. Phys. Chem. A* **101**, 3005 (1997).
- <sup>40</sup>B. Jayaram, Y. Liu, and D. J. Beveridge, *J. Chem. Phys.* **109**, 1465 (1998).
- <sup>41</sup>W. C. Still, A. Tempczyk, R. C. Hawley, and T. Hendrickson, *J. Am. Chem. Soc.* **112**, 6127 (1990).
- <sup>42</sup>A. Onufriev, D. Bashford, and D. Case, *J. Phys. Chem. B* **104**, 3712 (2000).
- <sup>43</sup>B. N. Dominy and C. L. Brooks, *J. Phys. Chem. B* **103**, 3765 (1999).
- <sup>44</sup>D. Bashford and D. Case, *Annu. Rev. Phys. Chem.* **51**, 129 (2000).
- <sup>45</sup>N. Calimet, M. Schaefer, and T. Simonson, *Proteins: Structure, Function, and Genetics* **45**, 144 (2001).
- <sup>46</sup>G. D. Hawkins, C. J. Cramer, and D. G. Truhlar, *Chem. Phys. Lett* **246**, 122 (1995).
- <sup>47</sup>G. D. Hawkins, C. J. Cramer, and D. G. Truhlar, *J. Phys. Chem.* **100**, 19824 (1996).
- <sup>48</sup>M. Schaefer and M. Karplus, *J. Phys. Chem.* **100**, 1578 (1996).
- <sup>49</sup>M. Feig, W. Im, and C. L. Brooks, *J. Chem. Phys.* **120**, 903 (2004).
- <sup>50</sup>M. S. Lee, J. F. R. Salsbury, and C. L. Brooks, III, *J. Chem. Phys.* **116**, 10606 (2002).
- <sup>51</sup>M. S. Lee, M. Feig, F. R. Salsbury, and C. L. Brooks, *Journal of Computational Chemistry* **24**, 1348 (2003).
- <sup>52</sup>A. Onufriev, D. Bashford, and D. A. Case, *Proteins* **55**, 383 (2004).
- <sup>53</sup>T. Wang and R. Wade, *Proteins* **50**, 158 (2003).
- <sup>54</sup>E. Gallicchio and R. M. Levy, *J. Comp. Chem.* **25**, 479 (2004).
- <sup>55</sup>H. Nymeyer and A. E. García, *Proc Natl Acad Sci U S A* **100**, 13934 (2003).
- <sup>56</sup>A. Ghosh, C. S. Rapp, and R. A. Friesner, *J. Phys. Chem. B* **102**, 10983 (1998).
- <sup>57</sup>M. Scarsi, J. Apostolakis, and A. Caffisch, *J. Phys. Chem. A* **101**, 8098 (1997).

- <sup>58</sup>W. Im, M. S. Lee, and C. L. Brooks, *Journal of Computational Chemistry* **24**, 1691 (2003).
- <sup>59</sup>U. Haberthür and A. Caffisch, *J Comput Chem* **29**, 701 (2007).
- <sup>60</sup>J. A. Grant, B. T. Pickup, M. J. Sykes, C. A. Kitchen, and A. Nicholls, *Phys. Chem. Chem. Phys.* **9**, 4913 (2007).
- <sup>61</sup>H. Tjong and H. X. Zhou, *J. Phys. Chem. B* **111**, 3055 (2007).
- <sup>62</sup>P. Labute, *Journal of Computational Chemistry* **29**, 1693 (2008).
- <sup>63</sup>A. Onufriev, D. A. Case, and D. Bashford, *Journal of Computational Chemistry* **23**, 1297 (2002).
- <sup>64</sup>A. V. Onufriev and G. Sigalov, *The Journal of Chemical Physics* **134**, 164104+ (2011), PMID: PMC3100913.
- <sup>65</sup>A. W. Lange and J. M. Herbert, *J. Chem. Theory Comput.* **8**, 1999 (2012).
- <sup>66</sup>C. Simmerling, B. Strockbine, and A. E. Roitberg, *J. Am. Chem. Soc.* **124**, 11258 (2002).
- <sup>67</sup>J. Chen, W. Im, and C. L. Brooks, *J Am Chem Soc* **128**, 3728 (2006).
- <sup>68</sup>H. Lei and Y. Duan, *J. Phys. Chem. B* **111**, 5458 (2007).
- <sup>69</sup>J. W. Pitera and W. Swope, *Proc Natl Acad Sci U S A* **100**, 7587 (2003).
- <sup>70</sup>A. Jagielska and H. A. Scheraga, *Journal of Computational Chemistry* **28**, 1068 (2007).
- <sup>71</sup>V. Hornak, A. Okur, R. C. Rizzo, and C. Simmerling, *Proc Natl Acad Sci U S A* **103**, 915 (2006).
- <sup>72</sup>R. E. Amaro, X. Cheng, I. Ivanov, D. Xu, and A. J. Mccammon, *Journal of the American Chemical Society* **131**, 4702 (2009).
- <sup>73</sup>J. Z. Ruscio and A. Onufriev, *Biophys. J.* **91**, 4121 (2006), PMID 1635688.
- <sup>74</sup>J. Chocholousová and M. Feig, *J. Phys. Chem. B* **110**, 17240 (2006).
- <sup>75</sup>W. Zheng, V. Spassov, L. Yan, P. Flook, and S. Szalma, *Computational Biology and Chemistry* **28**, 265 (2004).
- <sup>76</sup>J. Zhu, E. Alexov, and B. Honig, *The journal of physical chemistry. B* **109**, 3008 (2005).
- <sup>77</sup>A. V. Onufriev and D. A. Case, *Annual Review of Biophysics* **48**, 275 (2019).
- <sup>78</sup>D. L. Mobley and J. P. Guthrie, *Journal of Computer-Aided Molecular Design* **28**, 711 (2014).
- <sup>79</sup>D. L. Mobley, C. I. Bayly, M. D. Cooper, M. R. Shirts, and K. A. Dill, *Journal of Chemical Theory and Computation* **11**, 1347 (2015).

- <sup>80</sup>A. Mukhopadhyay, B. H. Aguilar, I. S. Tolokh, and A. V. Onufriev, *Journal of Chemical Theory and Computation* **10**, 1788 (2014).
- <sup>81</sup>D. A. Case et al., *Journal of Computational Chemistry* **26**, 1668 (2005).
- <sup>82</sup>M. Ramanadham, L. C. Sieker, and L. H. Jensen, *Acta Crystallographica Section B Structural Science* **46**, 63 (1990).
- <sup>83</sup>X. Wang, J. Lan, J. Ge, J. Yu, and S. Shan, Crystal structure of SARS-CoV-2 spike receptor-binding domain bound with ACE2, <https://www.rcsb.org/structure/6M0J>, 2020.
- <sup>84</sup>J. C. Gordon et al., *Nucleic Acids Research* **33**, W368 (2005).
- <sup>85</sup>M. L. Connolly, *Journal of Applied Crystallography* **16**, 548 (1983).
- <sup>86</sup>S. Decherchi and W. Rocchia, *PLoS ONE* **8**, e59744 (2013).
- <sup>87</sup>J. A. Grant, B. T. Pickup, and A. Nicholls, *Journal of Computational Chemistry* **22**, 608 (2001).
- <sup>88</sup>H. Tjong and H.-X. Zhou, *Journal of Chemical Theory and Computation* **4**, 507 (2008).
- <sup>89</sup>C. J. Cramer and D. G. Truhlar, *Accounts of Chemical Research* **41**, 760 (2008).
- <sup>90</sup>A. V. Onufriev and B. Aguilar, *Journal of Theoretical & Computational Chemistry* **13**, 1440006 (2014).
- <sup>91</sup>F. M. Richards, *Annual Review of Biophysics and Bioengineering* **6**, 151 (1977).
- <sup>92</sup>A. Bondi, *The Journal of Physical Chemistry* **68**, 441 (1964).
- <sup>93</sup>D. Bashford, An object-oriented programming suite for electrostatic effects in biological molecules An experience report on the MEAD project, in *Scientific Computing in Object-Oriented Parallel Environments*, edited by Y. Ishikawa, R. R. Oldehoeft, J. V. W. Reynders, and M. Tholburn, *Lecture Notes in Computer Science*, pages 233–240, Berlin, Heidelberg, 1997, Springer.
- <sup>94</sup>Y. C. Zhou, M. Feig, and G. W. Wei, *Journal of Computational Chemistry* **29**, 87 (2008).
- <sup>95</sup>A. Onufriev, D. Bashford, and D. A. Case, *Proteins: Structure, Function, and Bioinformatics* **55**, 383 (2004).
- <sup>96</sup>J. G. Kirkwood, *The Journal of Chemical Physics* **2**, 351 (1934).
- <sup>97</sup>A. T. Fenley, J. C. Gordon, and A. Onufriev, *The Journal of Chemical Physics* **129**, 075101 (2008).
- <sup>98</sup>G. Sigalov, A. Fenley, and A. Onufriev, *The Journal of Chemical Physics* **124**, 124902 (2006).

- <sup>99</sup>G. Sigalov, P. Scheffel, and A. Onufriev, *The Journal of Chemical Physics* **122**, 094511 (2005).
- <sup>100</sup>R. Cammi and J. Tomasi, *Journal of Computational Chemistry* **16**, 1449 (1995).
- <sup>101</sup>B. Honig, K. Sharp, and A. S. Yang, *The Journal of Physical Chemistry* **97**, 1101 (1993).
- <sup>102</sup>B. Aguilar and A. V. Onufriev, *Journal of Chemical Theory and Computation* **8**, 2404 (2012).
- <sup>103</sup>E. V. Katkova, A. V. Onufriev, B. Aguilar, and V. B. Sulimov, *Journal of Molecular Graphics and Modelling* **72**, 70 (2017).
- <sup>104</sup>S. Izadi, R. C. Harris, M. O. Fenley, and A. V. Onufriev, *Journal of Chemical Theory and Computation* **14**, 1656 (2018).
- <sup>105</sup>C. C. F. Blake et al., *Proceedings of the Royal Society of London. Series B. Biological Sciences* **167**, 378 (1967).
- <sup>106</sup>D. C. Phillips, *Scientific American* **215**, 78 (1966).
- <sup>107</sup>A. Warshel and M. Levitt, *Journal of Molecular Biology* **103**, 227 (1976).
- <sup>108</sup>Z. Li and T. Lazaridis, *Physical Chemistry Chemical Physics* **9**, 573 (2007).
- <sup>109</sup>S. B. de Beer, N. P. Vermeulen, and C. Oostenbrink, *Current Topics in Medicinal Chemistry* **10**, 55 (2010).
- <sup>110</sup>F. Spyrakakis et al., *Journal of Medicinal Chemistry* **60**, 6781 (2017).
- <sup>111</sup>D. Hamelberg and J. A. McCammon, *Journal of the American Chemical Society* **126**, 7683 (2004).
- <sup>112</sup>M. Petřek et al., *BMC Bioinformatics* **7**, 316 (2006).
- <sup>113</sup>I. S. Tolokh et al., *Nucleic acids research* **42**, 10823 (2014), PMID: PMC25123663.
- <sup>114</sup>J. Zahradník et al., *bioRxiv* , 2021.01.06.425392 (2021).